Shear-induced partial translational ordering of a colloidal solid

B. J. Ackerson
Department of Physics, Oklahoma State University, Stillwater, Oklahoma 74078

N. A. Clark
Department of Physics, University of Colorado, Boulder, Colorado 80303
(Received 16 January 1984)

Highly charged submicrometer plastic spheres suspended in water at low ionic strength will order spontaneously into bcc crystals or polycrystals. A simple linear shear orients and disorders these crystals by forcing (110) planes to stack normal to the shear gradient and to slide relative to each other with a ⟨111⟩ direction parallel to the solvent flow. In this paper we analyze in detail the disordering and flow processes occurring beyond the intrinsic elastic limit of the bcc crystal. We are led to a model in which the flow of a colloidal crystal is interpreted as a fundamentally different process from that found in atomic crystals. In the colloidal crystal the coupling of particle motion to the background fluid forces a homogeneous flow, where every layer is in motion relative to its neighboring layers. In contrast, the plastic flow in an atomic solid is defect mediated flow. At the lowest applied stress, the local bcc order in the colloidal crystal exhibits shear strains both parallel and perpendicular to the direction of the applied stress. The magnitude of these deformations is estimated using the configurational energy for bcc and distorted bcc crystals, assuming a screened Coulomb pair interaction between colloidal particles. As the applied stress is increased, the intrinsic elastic limit of the crystal is exceeded and the crystal begins to flow with adjacent layers executing an oscillatory path governed by the balance of viscous and screened Coulomb forces. The path takes the structure from the bcc_1 and bcc_2 twins observed at zero shear to a distorted two-dimensional hcp structure at moderate shear rates, with a loss of interlayer registration as the shear is increased. This theoretical model is consistent with other experimental observations, as well.

I. INTRODUCTION

Aqueous suspensions of uniformly sized submicrometer polymer spheres are model colloids.[1] The colloidal particles are highly charged and may interact over a long range such that even in dilute suspensions (0.1 wt. %) they exhibit interparticle solidlike or liquidlike order. Average particle separations may be adjusted so that light scattering can be used to investigate the collective colloidal-particle order. The equilibrium properties of these "colloidal solids" and "colloidal liquids" have been studied extensively, and experimental results illustrate the strong correspondence to pure fluids and solids in both structure and dynamics of equilibrium fluctuations.[2,3]

Recently there has been a growing interest in the microscopic and macroscopic properties of sheared spherical-particle systems.[2,4–8] Our earlier microscopic structure studies,[5–7] using light scattering from dilute colloidal suspensions, have revealed a variety of structures as the rate of shear is varied. When samples which spontaneously form body-centered cubic crystal (bcc) lattices in equilibrium[9] are subjected to increasing shear, they will pass through a series of structures before melting and finally exhibiting an amorphous or fluidlike order. This shear-induced melting is reversible and is not due to an increase in temperature, as the temperature remains well below that required for melting. Furthermore, the liquidlike structure exhibits a distortion in the pair distribution function, which corresponds to that anticipated for pure fluids at extreme rates of shear.[10]

This shear-induced melting phenomena also has been observed in more concentrated ($\sim 10\%$) aqueous suspensions by Pieranski,[2] in nearly close-packed suspensions by Hoffman,[8] and in solid argon by computer simulation by Evans.[11] Light scattering has been used by Pieranski and Hoffman to monitor the transition from sliding solid layers to an amorphous liquidlike structure as the rate of shear increases. The transition is accompanied by an abrupt increase in the shear viscosity (shear thickening).[8] By testing a variety of samples Hoffman has demonstrated that the instability leading to the transition has a universal character and may be related to microscopic parameters. Because this phenomena of shear-induced melting is observed in such a broad range of systems it may be more general than initially anticipated and merits closer examination.

Furthermore, molecular-dynamics studies suggest many similarities between the properties of colloidal suspensions sheared at modest rates and the properties of pure atomic systems, sheared isothermally at enormously large rates.[10,12] In Evans's[11,13] investigation of shear-induced melting, he finds that the stress tensor, which describes the pressures and viscosities of the system, evolves continuously as a function of the rate of shear. However, the tensor shows regions of different analytic behavior, which suggest different microscopic organization in different shear-rate regimes. He points out the similarity with the colloidal-suspension experiments and indicates that these

phenomena may provide an alternative to other theories of plastic flow, such as those used to describe Bingham plastics. Other results from nonequilibrium molecular dynamics suggest that system properties may not be expandable as an analytic function in the rate of shear. This effect may be related to the long time tail in the equilibrium velocity autocorrelation function[13] and/or nonlinear coupling effects.[14] Because there seems to be a strong analogy between colloidal solids and liquids with pure atomic solids and liquids, colloidal systems may prove useful in understanding these and other nonequilibrium phenomena.

Our earlier experiments[5] at large rates of shear indicate a phase for which there is no long-range order, a suspension structure which is liquidlike or amorphous. As the rate of shear is reduced, we observe the development of short-ranged translational order characterized by strings of uniformly spaced colloidal particles which are parallel to the direction of the local solvent velocity, $\hat{V}$. As the rate of shear is further reduced, an abrupt transition (transition I) is observed where the colloidal-particle strings condense into distorted two-dimensional close-packed (2D hcp) layers. This is a transition from short-ranged to two-dimensional order. The layers are parallel to $\hat{V}$, perpendicular to the shear $\hat{\nabla}$, and freely slip past one another. Between transition I and a transition at a lower shear rate (transition II), there is no correlation along $\hat{V}$ of layers separated along $\hat{\nabla}$. These structures are similar to that found in equilibrium liquid crystal phases of disk-shaped molecules. For this reason one may consider such structures as *shear-induced liquid crystal phases.*

In this paper we present experimental results and a theoretical interpretation for the development of long-range order below transition II. Here the correlation length along $\hat{\nabla}$ for translational ordering parallel to $\hat{V}$ is observed by light scattering to increase from zero at transition II to infinity at a transition at small applied stress, corresponding to the intrinsic bcc crystal yield stress. Hence the entire sequence of the above-mentioned shear-induced structures occur beyond the elastic limit or above the intrinsic yield stress of the bcc crystal. Our earlier experiments suggested this shear flow beyond the elastic limit below transition II is plastic flow of three-dimensional crystals, mediated by dislocation motion. Solitons were proposed to move perpendicular to $\hat{V}$ and $\hat{\nabla}$ and parallel to $\hat{e}$ (see Fig. 1). These solitons changed one bcc twin structure to the other as they propagated. The intervening region between the two twin structures was a three-dimensional hexagonal close-packed (3D hcp) structure. This model was supported by the observation of two distinct kinds of structures seen in the diffraction pattern for scattering from a sample in the rocking-cuvette cell. Here both the (strained) twin bcc and the 3D hcp structures have signatures in the diffraction patterns in this shear-rate regime. However, the experimental results to be presented in this paper are for a well-characterized velocity profile and do not exhibit multiple coexisting structures (other than strained bcc twins) in this shear-rate regime. Furthermore, the observed bcc twin structures are found to be described well theoretically in terms of the

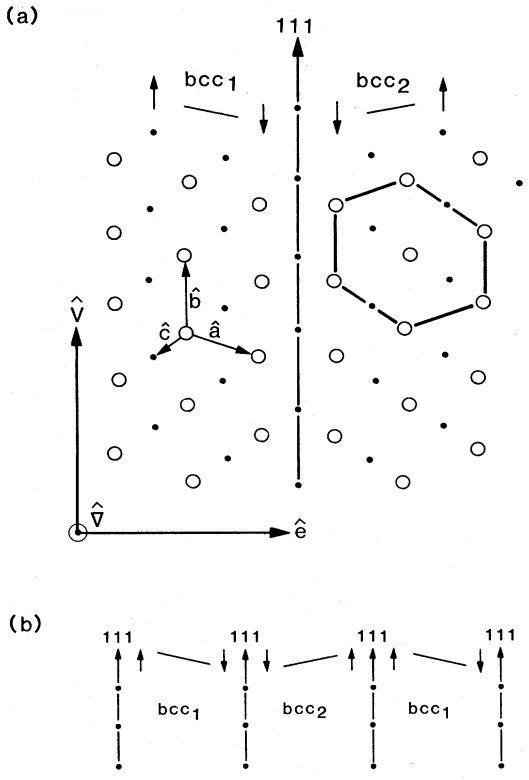

FIG. 1. Twin bcc structures (bcc_1 and bcc_2) are shown. In each structure a ⟨111⟩ direction is parallel to $\hat{V}$ and (110) planes are parallel to the $\hat{V}$-$\hat{e}$ plane. The common boundary between the twins is a (211) plane parallel to the $\hat{\nabla}$-$\hat{V}$ plane. (a) Two layers are shown. One is designated by ○ and the other by ●. Basis vectors $\vec{a}$, $\vec{b}$, and $\vec{c}$ are shown for the bcc lattice. The in-plane strain which changes these layers into a distorted 2D hcp or distorted fcc structures is shown by arrows for each twin. The transition being studied distorts the outlined hexagon into a more symmetrical hexagon. (b) Several bcc twins stacked in the $\hat{e}$ direction are shown. As the sample is stressed and flows, these structures oscillate as indicated by the arrows and exchange identities periodically. The (211) plane boundaries oscillate in the $\hat{V}$ direction.

continuous deformation of single bcc crystals which are stressed beyond the limit of stability. The stressed bcc crystal motion is coupled to the background fluid and the system follows an oscillatory path in strain space. At low shear this path takes the crystal from near the bcc twin structure through a distorted face-centered cubic (fcc) structure or distorted 2D hcp structure to near the other bcc twin structure. At moderate shear rates this path straightens to give distorted 2D hcp structures. This picture of colloidal crystal flow is quite distinct from normal plastic flow mechanisms of atomic crystals which are realized in terms of defect motion. In the colloidal crystal model the background fluid viscosity forces the whole crystal to homogeneously deform in response to the applied shear. This continuous deformation of the crystal results in a *flowing crystal.* We do expect plastic flow,

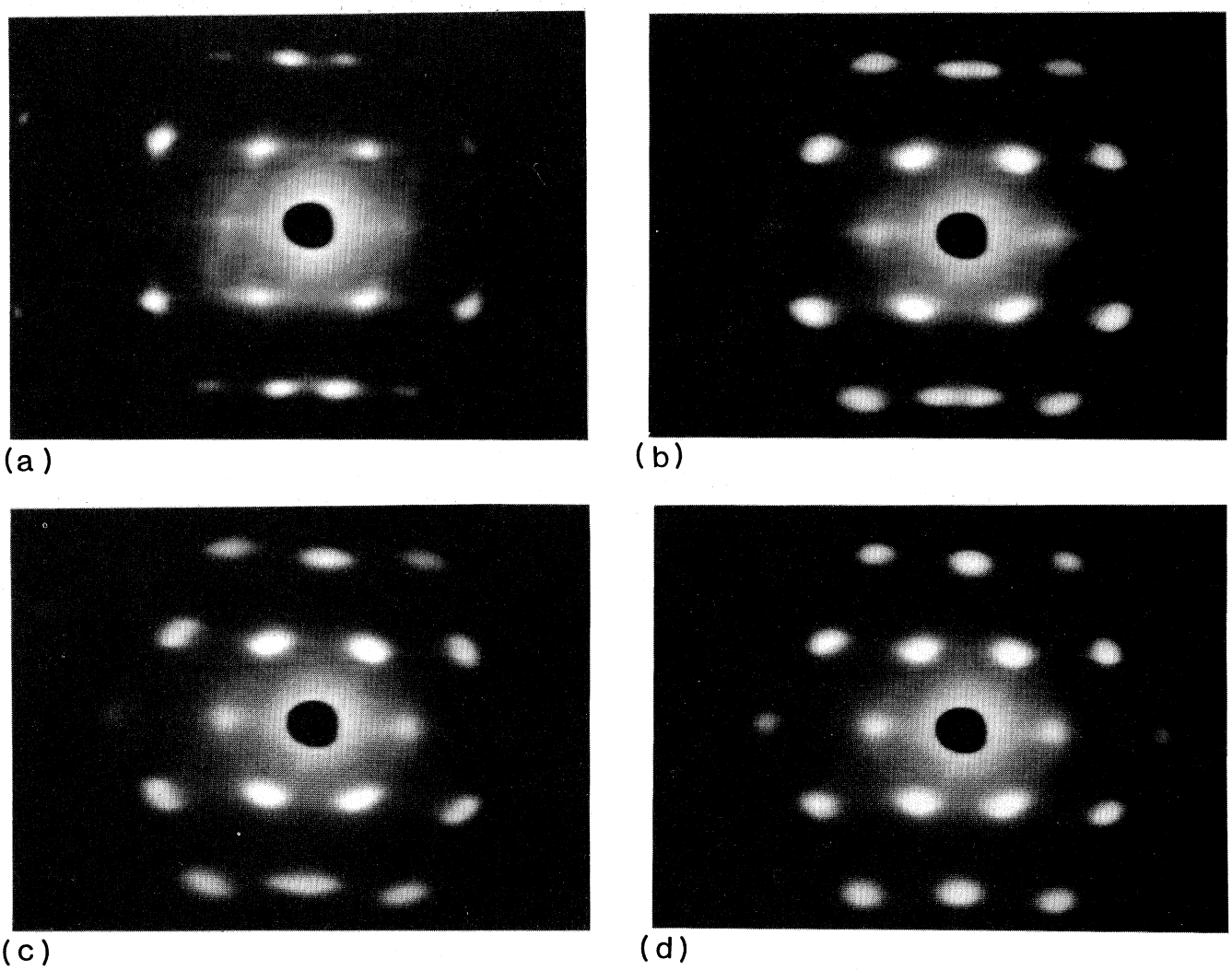

FIG. 2. Photographs of video records made of scattering intensity distributions produced by a 0.17 wt. % deionized aqueous suspension of 0.220-μm-diameter polystyrene particles. At zero shear a bcc twin structure is identified in (a). The visible lines are due to thermal diffuse scattering. For small rates of shear ($\hat{V}$ upward and $\hat{\nabla}$ normal to the plane of the page), the Laue spots are observed to shift horizontally toward a vertical axis, which passes through the k-space origin at the beam stop (center). This shift is proportional to the $\hat{k}_v$ component of a given reciprocal-lattice point and increases with increasing rate of shear. In (b) there are two sets of 211 spots, which have merged in (c) and continue to merge in (d) as the rate of shear is increased. In (d) the shear rate (~ 10 Hz) is sufficiently large that the original bcc structure now looks like a distorted 2D hcp structure.

however, at values of applied stress below the intrinsic bcc crystal yield stress, i.e., below those values investigated experimentally here and in our earlier studies.

In this paper we examine in detail the interparticle structure for rates of shear below transition II, from an equilibrium bcc solid to a collection of freely slipping distorted 2D hcp layers at moderate rates of shear (~ 10 Hz). We use an improved rotating-disk shear cell and are able to observe shear-induced distortions in the interparticle ordering. These distortions are measured as a function of the shear rate to study the continuity of the transition. Laser Doppler velocimetry is employed to measure flow profiles. These experimental details and results are reported in Sec. II.

II. EXPERIMENTAL DETAILS AND RESULTS

Earlier experiments employed either a rocking-cuvette cell, which has easy optical access but a time-dependent Poiseuelle flow profile, or a concentric-cylinder cell, which has less convenient optical access but a simple time-independent shear. The present rotating-disk cell consists of two quartz disks which are approximately 8 in. in diameter and separated by a uniform gap of ~ 1 mm. The total sample volume is 60 cc. One disk rotates at a steady but adjustable low rate of speed such that turbulence and radial flow effects are unimportant. The axle for rotation of the moveable disk is sealed by ~ 1-mm-thick teflon quad rings which contact the rotating disk

and cell wall. The outer portion of the cell is sealed by a silicon rubber *o*-ring which the stationary disk contacts. The incident laser beam ($\lambda=6328$ or 4880 Å) can be directed perpendicular to the plane of the gap between the disks, or rotated about this position by $\pm 60°$. This rotation can be made about an axis parallel to $\hat{V}$ or an axis parallel to $\hat{e}$.

The samples used in these studies are similar to those in previous experiments.[7] Aqueous suspensions of highly charged, Dow Chemical polystyrene, latex spheres (diameter $\cong 0.2\ \mu$m) are diluted to a concentration of ~ 0.1 wt. % and are highly deionized by addition of a strong acid-base mixed-bed ion exchange resin. The samples will form bcc polycrystalline structures after several days contact with the exchange resin. Experiments are conducted at room temperature without thermostating ($T=24 \pm 1$ °C).

If the colloidal sample sustains a shear flow which is gradually eliminated, macroscopic striations are observed which exhibit rapid submillimeter structure variation along $\hat{e}$ but are extended in the flow-velocity direction $\hat{V}$. Light scattering Laue patterns index to bcc structures and indicate the existence of two twin-related bcc crystals, as depicted in Fig. 1. A bcc ⟨111⟩ direction, the closest packed direction, is parallel to $\hat{V}$ and perpendicular to $\hat{\nabla}$. The bcc (110) planes, which slip over one another, are the closest packed planes. This close-packed orientation criteria corresponds to the preferred slip direction and slip planes in metals,[15] and it admits to the two possible twin bcc structures which are observed. Here, however, the solid polycrystalline structure not only slips in these preferred directions but also has been reoriented by the flow.

When the oriented bcc crystal sample is subjected to a shear stress, the observed scattered light Laue pattern distorts from that seen in equilibrium. This distortion may be seen in Fig. 2 which presents photographs of the observed scattering pattern as a function of the rate of shear for a sample illuminated with Ar^+ laser light ($\lambda=4880$ Å) incident normal to $\hat{V}$ and $\hat{e}$ (zero angle of incidence). The bcc 110 reciprocal-lattice points, connected by line segment *B* in Fig. 3, are observed to shift symmetrically towards a vertical axis passing through the reciprocal-lattice origin (beam-stop position) and parallel to $\hat{k}_v$. The bcc 211 reciprocal-lattice points, connected by line segment *A* in Fig. 3, also shift in the same way and those pairs closest to this vertical axis merge to become single spots at the end of this shear-induced evolution. The final scattering pattern looks less like that for a twin bcc structure and more like that for a distorted 3D fcc or 2D hcp structure which is compressed in the $\hat{V}$ direction. Quantitative measurements of the relative displacement of reciprocal-lattice points are presented in Fig. 3. Those relative separations, which change as a function of shear, show a discontinuous change from the equilibrium bcc position for a small but finite initial shear rate followed by a continuous evolution to the distorted hcp structure with increasing shear rate. This deformation is reversible. However, the relaxation from small but finite shear to the zero shear value takes ~ 1 h, whereas the other deformations are stable within seconds of a change in the rate of shear.

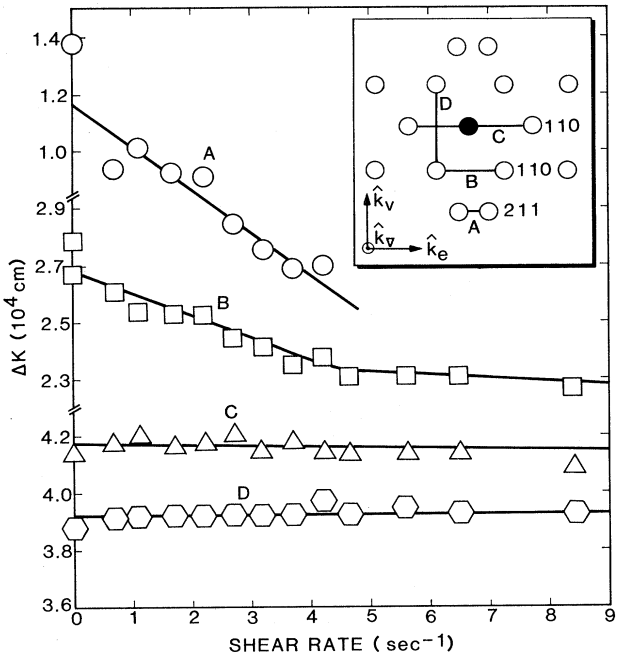

FIG. 3. Relative *k*-space separation for selected reciprocal-lattice points as a function of the rate of shear. The specific separations measured are depicted in the schematic scattering pattern shown in the upper right-hand corner. The horizontal displacement of a spot is seen to be proportional to the $\hat{k}_v$ component of the reciprocal-lattice point. That is to say, the slope of the *A* line is twice the *B* line, and the *C* line has zero slope. There is little relative displacement vertically. A discontinuous change in relative displacement occurs at small rates of shear; the equilibrium bcc positions do not merge continuously with the values obtained by extrapolating to zero shear. Extrapolation of the low shear-rate lines *A* and *B* give the proper *k*-space values for the distorted 2D hcp structure at the same large rate of shear.

While no quantitative intensity measurements have yet been made, the higher-order reciprocal-lattice points are diminished in intensity when the sample is sheared, and there is a variation in intensity between point pairs reflected about a vertical axis passing through the reciprocal-lattice origin and parallel to $\hat{k}_V$, and also for reflection through a horizontal axis parallel to k_e and passing through the reciprocal-lattice origin. As the angle of incidence of the probe beam is changed for the equilibrium bcc crystal, we observe spots in the scattering pattern to change in intensity, indicating that reciprocal-lattice points come on and off the Ewald sphere. This indicates that there is three-dimensional ordering. However, as the rate of shear is increased, this ordering in the $\hat{\nabla}$ direction becomes shorter ranged and the reciprocal-lattice points, except in the $\hat{k}_\nabla$-$\hat{k}_e$ plane ($\hat{k}_V=\hat{0}$), begin to extend as long tubes in the $\hat{k}_\nabla$ direction. In the $\hat{k}_\nabla$-$\hat{k}_e$ plane a bcc 110 reciprocal-lattice point remains fairly distinct and is brightest for all shear rates when the incident beam makes an angle $\theta=30°$ with respect to $\hat{k}_\nabla$ in the $\hat{k}_\nabla$-$\hat{k}_e$ plane.

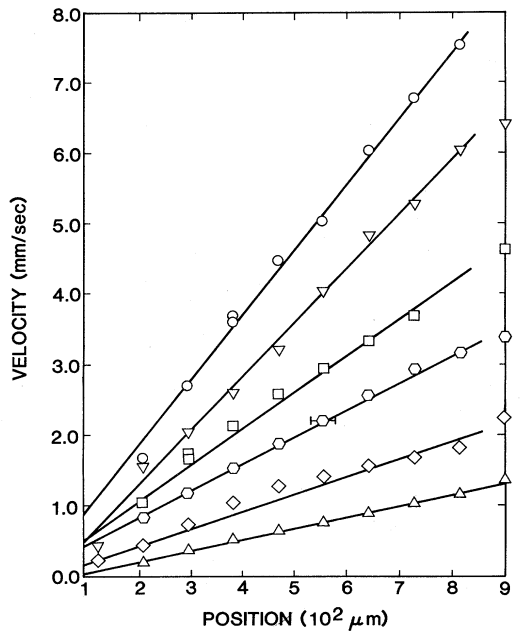

FIG. 4. Velocity profiles in the disk cell for several different rates of shear. All data indicate simple linear shear within experimental error. There is neither plug flow nor stationary crystal structure near the walls. The velocities reported for 900 μm are determined from measurements of the rotational speed of the moving disk.

Velocimetry measurements[16] were made sampling the 1 mm gap at approximately 100 μm intervals. Each velocimetry run lasted approximately 30—60 sec. Owing to geometrical constraints, the scattered wave vector was not parallel to the $\hat{V}$ direction; but the ratio of the components in the shear and velocity directions was $k_\nabla/k_v = \tan 39°$. The reported velocities in Fig. 4 represent a direct inference of the local velocity from the frequency of oscillation of the measured correlation function without correction for shear aliasing[16] or multiple scattering. The actual velocities are quite small and laminar flow with a constant shear is present under all experimental conditions. The velocities reported for 900 μm are determined from a direct measurement of the wall velocity and agree well with the light scattering results. There seems to be neither stationary crystal regions adhering to the walls producing a large shear in the region between the plates nor a plug flow having a low shear region in the center with a high shear near the walls.

III. INTERPRETATION

A. General considerations

The gross features of the observed phenomena are consistent with our shear experiments using the rocking-cuvette and rotating-cylinder cells. The basic transition from a twin bcc structure to a distorted two-dimensional sliding-layer structure is preserved. However, we do not observe the additional 3D hcp marker, the doubling of spots near the bcc 110 reciprocal-lattice point in the $\hat{k}_e$-$\hat{k}_\nabla$ plane, reported for the rocking-cuvette experiments. This phenomenon may be related to the more complex shear in the cuvette. Furthermore, we have observed an initially discontinuous behavior followed by a steady continuous deformation as the shear rate is increased from zero. These new results lead us to reexamine the processes at work at low rates of shear.

The shift of the observed spots or reciprocal-lattice points may be understood as a simple "in-plane" shear of the bcc (110) layers as is indicated by the arrows in Fig. 1. Such a deformation will produce a shift of reciprocal-lattice points in a direction having both $\hat{k}_\nabla$ and $\hat{k}_e$ components, and the shift will be proportional to the $\hat{k}_v$ component. Experimental measurements of the magnitude of the shift in the $\hat{k}_e$ direction are presented in Fig. 3. Note the dependence of the shift on the $\hat{k}_v$ magnitude of the spot pairs *A*, *B*, and *C*. Evidently, as the rate of shear is increased, each layer distorts until at the end of transition II it is symmetric and identical to its twin. This deformation, which does not change the spacing of particles in strings extended along $\hat{V}$ nor the spacing of strings along $\hat{e}$, produces a distorted 2D hcp structure like that observed in the scattering patterns at transition II. The real space-distorted structure is 8% shorter along the $\hat{V}$ direction than a true 2D hcp structure. Remarkably, this shear distortion is perpendicular to the shear direction $\hat{\nabla}$ and has the opposite sense in each of the twins. Furthermore, the constancy of the incident angle θ, at which the bcc 110 reciprocal-lattice point in the $\hat{k}_\nabla$-$\hat{k}_e$ plane maintains its maximum intensity, indicates that the separation between layers normal to $\hat{\nabla}$ is a constant (within 10%) as a function of the rate of shear. The decrease in intensity of higher-order reciprocal-lattice points indicates an effectively larger Debye-Waller factor or larger rms fluctuations in particle position about lattice sites. This is not surprising when one considers the violent nature of the shearing process. It is surprising that the system maintains a fairly regular homogeneous structure, as indicated by the reasonably simple scattering pattern with well-defined spots.

The intensity asymmetries in the Laue patterns presented in Fig. 2 may be due, in part, to effects of the in-plane shear discussed above, but may also indicate other shear deformations of the real lattice. These deformations can change the relative distance of reciprocal-lattice points from the Ewald sphere in this geometry in a nonsymmetric way. In addition to a shear within a layer in the $\hat{e}$ direction, there may be layer-stacking shears in the $\hat{\nabla}$ direction. These shears may be of two kinds: a staggering of layers in the $\hat{V}$ direction as one moves along $\hat{\nabla}$ and a staggering of layers in the $\hat{e}$ direction as one moves along $\hat{\nabla}$. These shears correspond to the expected shifts in a layer of marbles which is pushed over another layer with a zig-zag motion.

B. Strained bcc crystals

Because the equilibrium sample is an oriented bcc crystalline or polycrystalline state as shown in Fig. 1, we in-

vestigate the configurational energy of a single, oriented, three-dimensional, bcc crystal as a function of the strains suggested by light scattering experiments. To this end we must consider the colloidal-particle interactions. These particles are highly charged having a potential surface charge of $\sim 10^3 e$. However, the actual charge in solution is produced by partial dissociation of counterions from surface-bound sulfate groups. Also, counterions near the highly charged surface may condense.[17] The result of either of these processes is to reduce the effective charge for a given particle. Furthermore, the free counterions (uncondensed) act to screen the Coulomb interaction between particles.

Silva and Mokross[18] have computed the configurational energy per particle for colloidal particles interacting via screened Coulomb pair interactions. They find for sufficiently large screening lengths ($\kappa a \lesssim 2$, where κ is the inverse screening length and a is the bcc lattice constant) that the bcc crystal structure has the least configurational energy, compared to other lattices with the same density, particle charge, and κ. Thus the bcc structure should be the most stable at low temperatures. This is a generalization of the argument which demonstrates that a system of point particles, which interact via Coulomb repulsive interactions in a uniform neutralizing background of the opposite charge, will form a bcc crystal at low density and temperature. This is a "Wigner crystal"[19] and this term has also been used to describe the bcc crystal structure seen in the colloidal suspensions.[18,20,21] We use the Silva and Mokross approach to calculate the configurational energy per particle for different distortions of the bcc lattice. This energy is given by the following summation which converges extremely slowly for small κa:

$$\phi = \frac{Z^2 e^2}{\epsilon} \sum_{\{\vec{r}_i\}} \frac{e^{-\kappa |\vec{r}_i|}}{|\vec{r}_i|} . \tag{3.1}$$

Here Ze is the effective colloidal-particle charge, κ is the reciprocal screening length (excluding macroion charge), ϵ is the dielectric constant of the medium (~ 80 for water) and $\{\vec{r}_i\}$ are particle positions in the lattice excluding the reference particle at the origin. This summation may be broken into two highly convergent sums using the method of Ewald.[22] Here we make use of the integral transform used by Silva and Mokross,

$$\frac{\exp(-\kappa r)}{r} = \frac{2}{\sqrt{\pi}} \left[\int_0^{\delta} \exp(-r^2 t^2 - \kappa^2/4t^2) dt + \int_{\delta}^{\infty} \exp(-r^2 t^2 - \kappa^2/4t^2) dt \right] , \tag{3.2}$$

and the θ transformation connecting the real $\{\vec{r}_i\}$ and reciprocal lattices $\{\vec{k}_i\}$,

$$\sum_l \exp(-|\vec{r}-\vec{r}_l|^2 \tau^2) = \sum_m \frac{\pi^{3/2}}{L^3 \tau^3} \exp(i\vec{k}_m \cdot \vec{r} - k_m^2/4\tau^2) - \frac{1}{(2\pi)^3} \exp(-r^2\tau^2) , \tag{3.3}$$

where L^3 is the primitive lattice volume and $\vec{r}$ is any position in space, to find

$$\phi = \frac{Z^2 e^2}{\epsilon} \left\{ \sum_m \frac{4\pi}{L^3} e^{i\vec{k}_m \cdot \vec{r}} \left[\frac{\exp[-(\vec{k}_m^2 + \kappa^2)/4\delta^2]}{(\vec{k}_m^2 + \kappa^2)} \right] + \sum_l \frac{1}{2|\vec{r}-\vec{r}_l|} \left[e^{\kappa|\vec{r}-\vec{r}_l|} \operatorname{erfc}\left(|\vec{r}-\vec{r}_l|\delta + \frac{\kappa}{2\delta} \right) + e^{-\kappa|\vec{r}-\vec{r}_l|} \operatorname{erfc}\left(|\vec{r}-\vec{r}_l|\delta - \frac{\kappa}{2\delta} \right) \right] + \frac{1}{8\pi^3} \left[\kappa \operatorname{erfc}\left(\frac{\kappa}{2\delta} \right) - \frac{2}{\sqrt{\pi}} \delta \exp(-\kappa^2/4\delta^2) \right] \right\} . \tag{3.4}$$

The reciprocal-space terms result from using the θ transformation on the integral which extends over the range from 0 to δ. The integral from δ to ∞ is performed without use of the θ transformation. The Ewald parameter δ is adjustable to give optimal convergence and may be set equal to the reciprocal of the bcc lattice constant, $\delta = 1/a$. To find the potential energy of the reference particle at the origin, one simply sets $\vec{r} \equiv 0$ and excludes this point ($\vec{r}_l = 0$) from the sum, as has been done already for the θ transformation. While this calculation is identical to that of Silva and Mokross, we present the final result in Eq. (3.4), because the form is a simplified version of their result and is more easily programmed for computation. We have not included the energy of the counterion cloud of the particle at the origin. This will lead to a divergence of our result as $\kappa a \to 0$. Inclusion of this term leads to an extra term dependent on κa in Eq. (3.4) and gives numerical results identical to those of Silva and Mokross. However, as long as we make lattice distortion comparisons at the same κa value, this term is not important. Also, if we are interested in forces or differences in potential at a given κa, this term produces no effect.

Distortions of the bcc crystal are studied by using the following basis vectors to generate the bcc lattice:

$$\vec{a}'=\vec{a}-\delta_2\vec{b}\,,$$
$$\vec{b}'=\vec{b}\,, \tag{3.5}$$
$$\vec{c}'=\vec{c}+\delta_3\vec{b}+\delta_1\left[\vec{a}-\frac{\vec{a}\cdot\vec{b}}{b^2}\vec{b}\right],$$

where

$$\vec{a}=\frac{a}{2}(\hat{x}+\hat{y}-\hat{z})\,,$$
$$\vec{b}=\frac{a}{2}(-\hat{x}+\hat{y}+\hat{z})\,, \tag{3.6}$$
$$\vec{c}=\frac{a}{2}(\hat{x}-\hat{y}+\hat{z})\,.$$

Here $\hat{x}$, $\hat{y}$, and $\hat{z}$ are mutually orthogonal unit vectors and $\vec{a}$, $\vec{b}$, and $\vec{c}$ are the basis vectors for a perfect bcc lattice. The velocity vector $\hat{V}$ for this particular bcc orientation may be taken parallel to $\vec{b}$. The vectors $\vec{a}$ and $\vec{b}$ are basis vectors for the bcc (110) plane shown in Fig. 1. The basis vectors for a distorted bcc lattice are given by $\vec{a}'$, $\vec{b}'$, and $\vec{c}'$, where shear strains are introduced into the perfect bcc structure through the δ parameters. The experimentally observed shear of the (110) plane indicated in Fig. 1 is generated by δ_2. Stacking distortions are produced by δ_3 for staggering layers in the $\hat{V}$ direction and by δ_1 for staggering layers in the $\hat{e}$ direction. These distortions preserve the crystal density, the distance between particles in a string, and the distance between strings in the $\hat{V}$-$\hat{e}$ plane.

Basis vectors of the reciprocal lattice must be generated from $\vec{a}'$, $\vec{b}'$, and $\vec{c}'$ if the sum in Eq. (3.4) is to be performed. To this end we find the following reciprocal-lattice vectors for the distorted bcc lattice:

$$\vec{k}_a=\frac{2\pi}{a}[(1-\delta_1)\hat{x}+\hat{y}-\delta_1\hat{z}]$$
$$=\frac{2\pi}{a}\left[\frac{1}{\sqrt{2}}(1-2\delta_1)\hat{k}_\nabla+\left[\frac{3}{2}\right]^{1/2}\hat{k}_e\right],$$
$$\vec{k}_b=\frac{2\pi}{a}[(-\delta_1/3+\delta_2-\delta_3-\delta_1\delta_2)\hat{x}$$
$$+(1+\delta_2)\hat{y}+(1-\delta_1/3-\delta_3-\delta_1\delta_2)\hat{z}]$$
$$=\frac{2\pi}{a}\left[\frac{1}{\sqrt{2}}(1-2\delta_1/3+\delta_2-2\delta_3-2\delta_1\delta_2)\hat{k}_\nabla\right.$$
$$\left.+\frac{2}{\sqrt{3}}\hat{k}_v+\frac{1}{\sqrt{6}}(1+3\delta_2)\hat{k}_e\right], \tag{3.7}$$
$$\vec{k}_c=\frac{2\pi}{a}(\hat{x}+\hat{z})=\frac{2\pi}{a}(\sqrt{2}\hat{k}_\nabla)\,.$$

Note that the only shift parallel to the $\hat{k}_e$ direction is produced by δ_2, the in-plane shear. Also the magnitude of the shift will depend on the value of the $\hat{k}_v$ coordinate of the reciprocal-lattice point, as both the shift and the coordinate are associated with $\vec{k}_b$ only.

The configurational energy ϕ is calculated as a function of δ_2 and δ_3 by adjusting δ_1 to minimize ϕ for each pair of fixed values of δ_2 and δ_3. The results of this calculation for $\kappa a=1.0$ are presented schematically in Fig. 5. Here δ_2 measures in-plane distortions of (110) layers and $\delta_4=\delta_3-\delta_2/2$ measures the relative slip of adjacent (110) layers parallel to $\vec{b}$, when both displacement and distortions are taken into account. It is seen that this energy surface as a function of these variables has an hcp structure, which is compressed by 13% in the δ_4 direction compared to a perfect hcp structure. The peaks in this energy surface correspond to hexagonal structures (c axis parallel to $\hat{V}$) and have the largest configurational energy. The lowest energy points correspond to two twin bcc structures having the experimentally observed orientation. We define the energy of these structures to be zero. The saddle point on a line connecting two adjacent twin structures has a distorted fcc structure. The line $\delta_2\cong\frac{1}{6}$ intersects a subset of these saddle points and represents an in-plane shear which has brought the (110) layers into the more symmetric but distorted 2D hcp form, which is observed at the end of the shear-induced transition II. Thus, in equilibrium, the system sits in one of the low energy

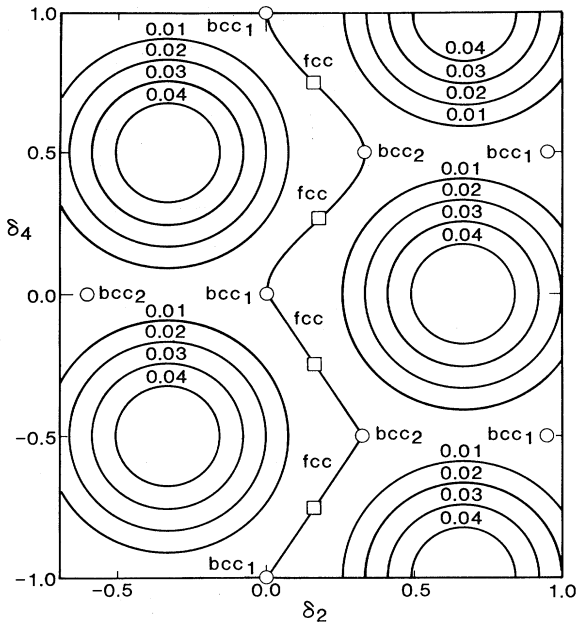

FIG. 5. Schematic drawing of the configurational energy $\epsilon a\phi/Z^2e^2$, for a distorted bcc lattice of colloidal particles, which interact via a screened Coulomb interaction with $\kappa a=1.0$. The energy surface has a distorted 2D hcp structure as a function of the shear-strain variables δ_2 and δ_4, which are defined in the text. The energy is defined to be zero for the perfect bcc twin structures (○) and is larger than zero for all other positions. Distorted fcc structures (□) are found at the midpoint of straight lines connecting adjacent bcc twin structures. A line for which $\delta_2=\frac{1}{6}$ corresponds to layers which have a distorted 2D hcp structure. The curved lines connecting bcc twin sites represent a trajectory for which $(\partial\phi/\partial\delta_2)=0$. The surface has qualitatively the same structure for $\delta_1=0$ or for δ_1 which minimizes ϕ.

bcc configurations. As the shear rate increases from zero, the system evolves to a region near the $\delta_2 \cong \frac{1}{6}$ line.

The configurational energy ϕ has been examined in detail along a straight line ($\delta_4 = 3\delta_2/2$) connecting two adjacent bcc twin sites for κa values in the range [0,2], the range of stability of the screened Coulomb bcc crystal. Figure 6 shows the change in the potential as a function of δ_4 for several values of κa. For each κa series, a constant is added so that all energies are zero in the bcc configuration. Surprisingly the resulting configurational energies are all quite similar and diminish only by 25% in maximum value as κa increases from $\kappa a = 0$ to 2.

By generalizing the method of Silva and Mokross, calculations have also been made for a crystal which has a finite number of (110) layers stacked in the shear direction $\hat{\nabla}$. The same shear strains given by the δ parameters are employed and the configurational energy is found to be nearly identical to that for the corresponding infinite crystal. The bcc configurations have the least energy and are the most stable equilibrium structure down to isolated systems of three layers. However, for isolated two- or one-layer systems the energy surface is quite different and the configurational energy of the distorted 2D hcp structure have the least value.

Calculations of the configurational energy have also been made for δ_1 constrained to zero. The structure of the energy surface presented in Fig. 5 is substantially the same. The bcc energies are identical. The difference between the bcc energy and the maximum energy of the surface changes by less than 10%. However, along the least-energy path connecting adjacent twin bcc structures, the maximum energy for the constrained calculation is three times that for the unconstrained calculation. Thus, if δ_1 does not relax to a minimum energy, the energy barrier between bcc twin sites is increased threefold.

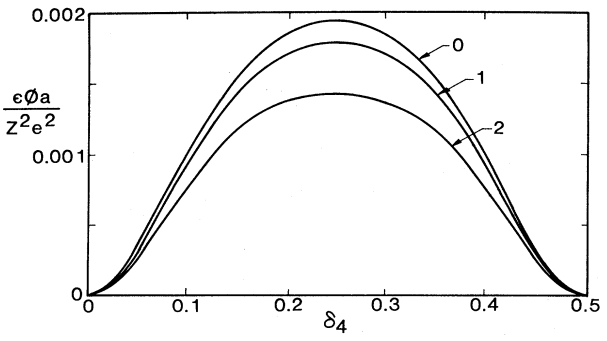

FIG. 6. Configurational energy $\epsilon a \phi / Z^2 e^2$ for a distorted bcc lattice of colloidal particles evaluated along a straight line connecting adjacent twin sites. The results are presented as a function of $\delta_4 (= 1.5\delta_2)$ for several values of κa. The qualitative structure is similar in all cases and the barrier height drops by 25% over the range of stability for bcc crystals (κa in the range [0,2]). The potential minima, defined to be zero, correspond to bcc twin sites. The maximum corresponds to a distorted fcc or distorted 2D hcp layer structure.

C. Model calculations

Because the configurational energy surface for a range of $\kappa a (= 0$ to 2) and different δ_1 constraints has essentially the same structure as a function of δ_2 and δ_4, we adopt the following mathematical model for $\phi(\delta_2, \delta_4)$:

$$\phi(\delta_2,\delta_4) = A\{\cos[2\pi(\delta_2 - \tfrac{2}{3})] + \cos[-\pi(\delta_2 - \tfrac{2}{3}) + 2\pi\delta_4] + \cos[-\pi(\delta_2 - \tfrac{2}{3}) - 2\pi\delta_4] + \tfrac{1}{2}\} . \quad (3.8)$$

This potential-energy surface has the same distorted hcp structure as that in Fig. 5. (Rescaling δ_4 by a factor $\sqrt{3}/2$ will bring this into a true hcp structure as a function of the variables.) The stresses or force per particle required to produce strains described by this potential may be calculated from ϕ by differentiation subject to the constraints of the problem. If a stress is applied to produce a strain δ_4 without any additional stresses to constrain δ_2, a path will be followed for which $(\partial\phi/\partial\delta_2)\,|_{\delta_4} = 0$. The system adjusts so that no additional strains are required to hold a particular value of δ_2. The configurational energy can be found along this path. The required stress or force per particle to produce this strain can then be found by differentiation of ϕ with respect to δ_4 along this path. The path for this motion is shown in the upper portion of Fig. 5 and is labeled by *I* in Fig. 7. In Fig. 8 the potential energy and force per particle for this motion are displayed. The energy is minimum in the bcc and twin bcc structures. It is maximum in the 3D fcc (distorted 2D hcp) structure. The force per particle is zero at all of these points and maximum for $\delta_4 = 0.12$. For small stresses the bcc crystal distorts and begins to shift from the energy minimum. As the stress is increased the distortion increases, until the stress exceeds the maximum restoring force at $\delta_4 = 0.12$. At this point the crystal fractures and slips or flows. Since we observe a linear shear profile in our experiments (without plug flow or crystals sticking to the walls of the cell), we conclude that the observed structure is a flowing structure. It exists beyond the limit of stability of the crystal. It should be noted, however, that slip or fracture in ordinary solids occurs for stresses much lower than that implied by these theoretical considerations.[15] This is thought to be due to thermally induced defects which provide another mechanism for deformation. Indeed, our earlier explanation for this phenomena is based on propagating solitary waves or defects in the crystal. However, this point of view has not yielded as rich an explanation of the data as the model to be developed.

Consider a colloidal crystal which flows when subjected to a shear stress. The relative motion of bcc (110) layers, which are parallel to the $\hat{e}$-$\hat{V}$ plane and move parallel to $\hat{V}$, is described by δ_4. A nonzero internal stress, which moves δ_4 away from the bcc minima, must be compensated by either a drag produced by the solvent or a stress applied by the walls of the container, or on acceleration results. However, we assume that the system is overdamped by the solvent forces so that acceleration terms are negli-

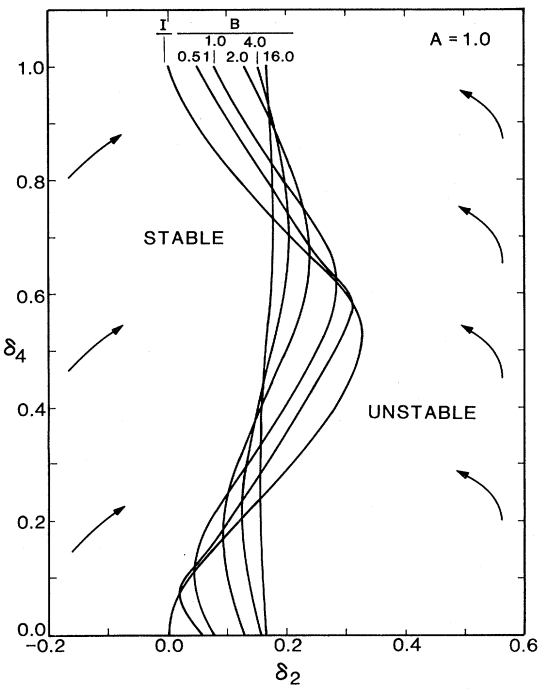

FIG. 7. Trajectories in δ_2-δ_4 strain space for $\mathscr{A}=1.0$ and various $\mathscr{B}$ values in the model potential calculations discussed in the text. For $\mathscr{B}\geq 0.5$ an initial starting point where δ_2 is in the interval $(-\frac{1}{3},\frac{2}{3})$ will produce a trajectory which decays to a stable orbit that oscillates about $\delta_2=\frac{1}{6}$. This represents a flowing crystal. For $\mathscr{B}\leq 0.5$ an arbitrary initial starting point will decay to a single point representing a static strain of the crystal. For $\delta_2=-\frac{1}{3}$ and $\frac{2}{3}$ there are unstable trajectories. Also shown is the trajectory for $(\partial\phi/\partial\delta_2)=0$ and is labeled I.

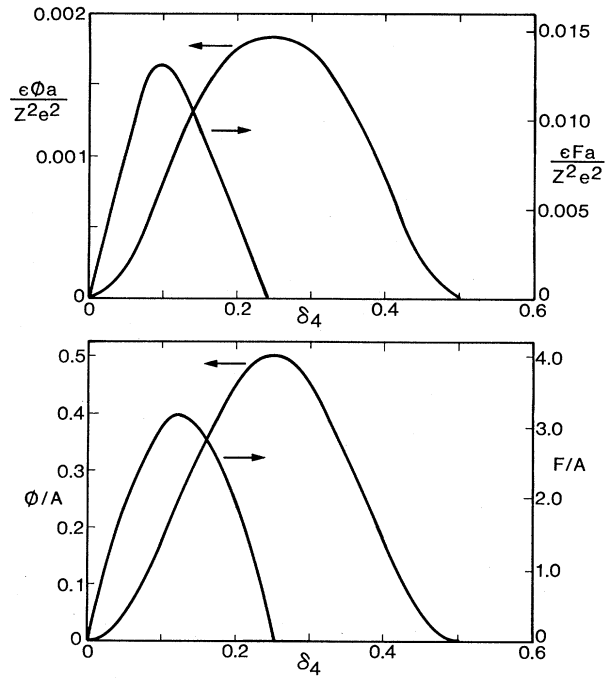

FIG. 8. A comparison is presented for the distorted bcc screened Coulomb potential $\epsilon a\phi/Z^2e^2(\kappa a=1.0)$ and the model potential ϕ/A along a path for which $(\partial\phi/\partial\delta_2)=0$ in each crystal. This path is near that taken by the experimentally sheared system. The force per particle required to produce the δ_4 distortion and overcome the potential barrier is also presented $[\epsilon aF/Z^2e^2=\partial(\epsilon a\phi/Z^2e^2)/\partial\delta_4$ and $F/A=\partial(\phi/A)/\partial\delta_4]$. The potentials are minimal at bcc twin structures (defined to be zero) and maximum at a distorted fcc or distorted 2D hcp structure. The forces are largest near $\delta_4\cong 0.1$ and represent the maximum strain that the crystal can withstand along this path.

gible. With this approximation in mind, we write the following equation of motion for δ_4:

$$\Gamma\dot{\delta}_4=\Gamma u-\frac{1}{|\vec{b}|}\frac{\partial\phi}{\partial\delta_4}+F\,. \tag{3.9}$$

Here we take $\Gamma=6\pi\eta s(a/\sqrt{2})$, where Γ is the drag coefficient per particle, η is the solvent viscosity, and s is the particle radius. The relative solvent velocity between adjacent layers parallel to the $\hat{e}$-$\hat{V}$ plane is given by $au/\sqrt{2}$. When u is not zero, there is a drag-induced stress on the particles in the crystal. In the absence of other forces, the layers will flow with the local solvent velocity. However, $-(1/|\vec{b}|)\partial\phi/\partial\delta_4$ gives the reaction force per particle in the $\hat{V}$ direction as a function of δ_4 (and δ_2) when the crystal is strained. Finally F gives the force per particle produced by interaction of the crystal with the container walls. For a statically strained crystal, $\dot{\delta}_4=0$, $u=0$, and the force applied to the edge of a perfect crystal produces a homogeneous strain throughout. Each particle in each layer is strained from its equilibrium position and produces a small reaction force. This force, when added to the forces produced by the other particles, balances the applied force. In this case F is opposite and equal to the reaction force per particle.

We must consider another equation of motion, because δ_4 and δ_2 are not independent. A stress, which changes δ_4, can also induce a change in δ_2, a strain which describes the in-plane shear of those (110) layers parallel to the $\hat{e}$-$\hat{V}$ plane. As the layer undergoes an in-plane shear, different parts of it will move with different velocities relative to the local solvent velocity of the layer. Those particles which are at rest with respect to the local solvent will feel no drag, while the drag on the other portions of the layer will increase linearly with distance from the line of zero drag. If we calculate the drag force per particle which damps the in-plane motion, we see that this force increases with the extent of the layer in the $\hat{e}$ direction. In an infinite layer, this is an infinite force and no δ_2 motion would be seen. Yet, it is the motion of δ_2 which is observed experimentally. Thus, the internal stresses produced by the δ_2 motion may cause a breakup of the infinite bcc crystal into strips of bcc twin structures which share common (211) boundary planes. These planes are parallel to the $\hat{V}$-$\hat{\nabla}$ plane and are the natural twinning planes in bcc metals.[23] An example of this structure is presented in Figs. 1(a) and 1(b) where the lines giving the [111] direction are also the edges of (211) planes separating two twin structures. In the presence of a shear each strip of crystal will oscillate between the two twin struc-

tures, alternate strips will be alternate twins, and the (211) boundary plane will oscillate parallel to $\hat{V}$ has shown in Fig. 1(b). The width of these twin structures in the $\hat{e}$ direction will determine the maximum drag force produced by changes in δ_2. This modification of the single crystal analysis maintains much of its content, removes the infinite drag problem, and forms a basis for understanding the striations observed experimentally.

The equation of motion for δ_2 in the overdamped limit is given by

$$\Gamma'\dot{\delta}_2 = -\frac{1}{|\vec{b}|}\frac{\partial\phi}{\partial\delta_2} + F' . \tag{3.10}$$

Here Γ' is the effective drag per particle and depends on the crystal width. No estimate of its value is given at this time. The reaction force per particle of the crystal structure is given by $-(1/|\vec{b}|\,\partial\phi/\partial\delta_2)$, where we assume ϕ is still given by the infinite crystal form. F' represents the forces applied by the walls of the container. The solvent velocity is the same everywhere within a given layer and therefore it does not enter as a factor in this equation.

The forces F and F' exerted by the container walls on the crystal are taken to be constant and equal to their time-averaged values. If F' is not zero by symmetry arguments, it will certainly oscillate about zero. Therefore, it is set equal to zero. The value for F is constrained because the velocimetry data indicates that the average local velocity in the colloidal structure is the same as the local velocity in the solvent. There is no unusual flow, no plug flow, nor any crystals sticking to the walls. Therefore, $\langle\dot{\delta}_4\rangle = u$ and we find the average value of F to be $F = (1/|\vec{b}|)\langle\partial\phi/\partial\delta_4\rangle$, where the brackets represent time averages.

If the form for ϕ presented in Eq. (3.8) is used to calculate the forces per particle in the equation of motion, we have

$$-\frac{\partial\phi}{\partial\delta_4} = 2\pi A\{\sin[-\pi(\delta_2-\tfrac{2}{3})+2\pi\delta_4] + \sin[\pi(\delta_2-\tfrac{2}{3})+2\pi\delta_4]\} = 2\pi A f_4 \tag{3.11}$$

and

$$-\frac{\partial\phi}{\partial\delta_2} = 2\pi A\{\sin[2\pi(\delta_2-\tfrac{2}{3})]+\tfrac{1}{2}\sin[\pi(\delta_2-\tfrac{2}{3})-2\pi\delta_4] + \tfrac{1}{2}\sin[\pi(\delta_2-\tfrac{2}{3})+2\pi\delta_4]\} = 2\pi A f_2 . \tag{3.12}$$

The equation for trajectories in δ_4-δ_2 space may then be found from a ratio of the two equations of motion, (3.9) and (3.10), as follows:

$$\frac{d\delta_4}{d\delta_2} = \mathscr{A}\left[\frac{\mathscr{B}+f_4}{f_2}\right], \tag{3.13}$$

where $\mathscr{A} = \Gamma'/\Gamma$ and $\mathscr{B} = |\vec{b}|(\Gamma u + F)/2\pi A$. Thus trajectories may be parametrized in terms of $\mathscr{A}$ and $\mathscr{B}$. A sample of trajectories has been computed numerically and is presented in Fig. 7 for $\mathscr{A}=1$ and various values of $\mathscr{B}$. Here a system started for any value of δ_2 in the range $(-\frac{1}{3},\frac{2}{3})$ will decay to a stable periodic orbit about $\delta_2=\frac{1}{6}$. An increase in the rate of shear corresponds to an increase in $\mathscr{B}$. As $\mathscr{B}$ increases, the trajectories become progressively more straight and close to $\delta_2=\frac{1}{6}$ for all values of δ_4. The maximum deviation of a trajectory from $\delta_2=\frac{1}{6}$ shifts to larger δ_4 as $\mathscr{B}$ increases. For $\mathscr{B} \lesssim \frac{1}{2}$ there are no stable periodic trajectories. A given starting position will decay to a point in the δ_4-δ_2 space and this represents a nonflowing distortion of the bcc crystal.

Physically the crystal is strained for low values of $\mathscr{B}$ but flows for large values. If the rate of flow is not too large the system can have significant in-plane relaxation of the (110) layers to produce distorted bcc structures. As the rate of shear increases, the in-plane distortion is limited by solvent drag forces and the trajectory tends to the $\delta_2=\frac{1}{6}$ line.

The speed of a point along a trajectory is given by

$$v(\delta_4,\delta_2) = \frac{2\pi A}{\Gamma'|\vec{b}|}[f_2^2+(\mathscr{B}+f_4)^2\mathscr{A}^2]^{1/2} \tag{3.14}$$

and is inversely proportional to the probability for finding the system in a given state of distortion. Normalized probability distributions are presented in Fig. 9 for some of the trajectories presented in Fig. 7. These distributions are presented as a function of δ_4 from which the value of δ_2 must be inferred. For $\mathscr{B} \lesssim \frac{1}{2}$ the distribution functions are δ functions representing single unique states. As $\mathscr{B}$ increases above $\frac{1}{2}$, the probability becomes continuously distributed having peaks where the crystal force is strong

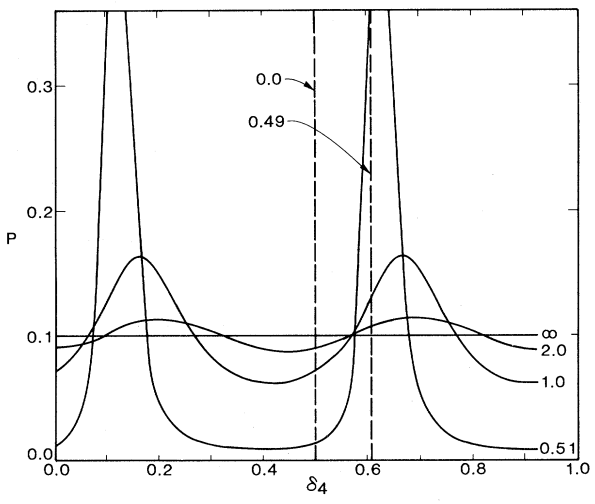

FIG. 9. Probability density P for finding the model colloidal solid in a given state of distortion as a function of δ_4 and parametrized by $\mathscr{B}$. For $\mathscr{B} \leq 0.5$ the system is static with one strain state for each $\mathscr{B}$ value. For $\mathscr{B} \geq 0.5$ the system flows and has a continuum of possible strain states. The largest probability for a given $\mathscr{B}$ corresponds to the state of greatest resistance to flow along a given trajectory. As the rate of shear increases ($\mathscr{B}$ increases) the probability becomes more uniformly distributed over the trajectory and the system becomes more two dimensional in character.

and retards the motion. For large shear the probability becomes uniformly distributed. The evolution from a peaked to a uniform distribution function is also observed experimentally. The reciprocal-lattice points of the bcc structure elongate continuously into tubes of light parallel to $\hat{k}_\nabla$ for $\vec{k}_v \neq 0$ as the rate of shear is increased. The tubes simply represent the multiplicity of structures implied by the probability distribution and are responsible for the scattering seen. Because the probability distribution can be calculated for a given trajectory in this model, the time-averaged reaction forces of the crystal may also be calculated. The force $F' = (1/|\vec{b}|)\langle \partial\phi/\partial\delta_2 \rangle$ is trivially zero because the trajectories are periodic. It is zero by assumption, otherwise. The force $F = (1/|\vec{b}|)\langle \partial\phi/\partial\delta_4 \rangle = -2\pi A f_4$ is presented in Fig. 10 as a function of $\Gamma u |\vec{b}|/2\pi A$ for $\mathscr{A} = 1$. Here the definition of $\mathscr{B}$ has been used in conjunction with $F = (1/|\vec{b}|)\langle \partial\phi/\partial\delta_4 \rangle$ to determine $\Gamma u |\vec{b}|/2\pi A$.

Now that the shear rate has been related to $\mathscr{B}$ and the probability distribution as a function of $\mathscr{B}$ is known, the most probable distortion δ_2 can be found as a function of shear. This result for our model with $\mathscr{A} = 1$ is presented in Fig. 10. At zero shear the distortion represents that for a bcc crystal. For infinitesimal rates of shear there is a discontinuous jump from the exact bcc value to values which produce distorted bcc structures. As the rate of shear is increased, δ_2 evolves continuously to a value consistent with the distorted 2D hcp structure. These model results are consistent with experimental observation.

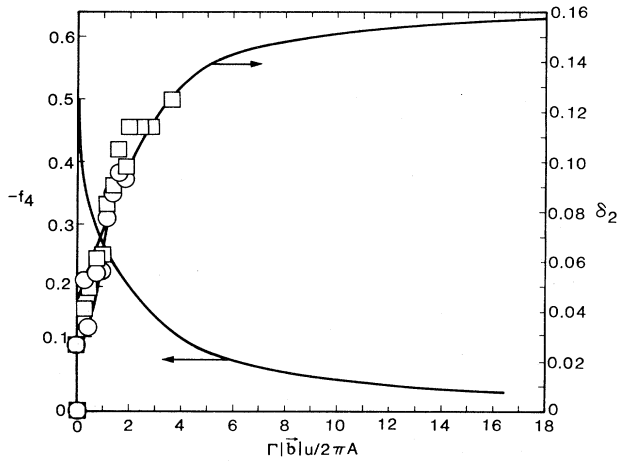

FIG. 10. The scaled force of resistance to flow $-f_4 = (1/2\pi A)\langle \partial\phi/\partial\delta_4 \rangle$ per particle is presented as a function of the scaled shear $\Gamma u |\vec{b}|/2\pi A$. The force decreases with increasing shear and indicates that the colloidal flow is shear thinning. Also shown is the most probable distortion (upper curve) and minimum distortion (lower curve) for δ_2 as a function of the rescaled shear. Note the discontinuous behavior between zero and finite values of shear. The experimental data has been fit to this model calculation, as shown, by adjusting the particle charge to $Z \cong 360$ to give a reasonable fit.

IV. DISCUSSION

In this paper we report experimental observations of the low shear-rate order induced in shear-oriented bcc colloidal crystals. At zero shear, oriented bcc twin structures coexist in suspension and macroscopic striations are observed. For small nonzero rates of shear the structure deforms discontinuously to a (time-averaged) distorted bcc twin structure. For increasing rates of shear, this distorted bcc structure evolves continuously into a distorted 2D hcp structure.

The data is interpreted on the basis of shear distortions of a bcc crystal lattice and a deterministic mechanical model of overdamped collective particle motion. The flowing structure is viewed as alternating layers of deforming twin bcc crystals stacked in a direction perpendicular to both the shear and velocity directions. This structure is tentatively identified with the experimentally observed striation. The shear flow causes these crystals to oscillate between the two different twin structures. For small rates of shear there is sufficient time for the crystals to relax that a distorted bcc twin structure can be identified from light scattering studies. However, the relaxation is not infinitely fast and there is a discontinuous jump between the zero shear and finite shear scattering patterns. As the rate of shear increases there is even less time to relax and the crystal adopts a structure halfway between the two twin structures, a distorted 2D hcp structure. The strain in the velocity direction becomes uniformly distributed in time and the light scattering exhibits more of a two-dimensional behavior.

While this model does involve edge dislocations which form the boundaries between the twin bcc structures, it is not the expected defect-assisted motion associated with plastic flow. We do expect plastic flow at applied stresses below those used in our experiments. The alternation between the two bcc twins should not be considered a Martensitic transition,[15] because it is not thermodynamically driven. Furthermore, Martensitic transitions generally involve a volume change (shear and compression) while these colloidal samples show only shear distortions. The structure referred to as the distorted fcc structure has an energy larger than the undistorted equal-density fcc structure, the equilibrium structure for $\kappa a \geq 2$. This undistorted fcc structure cannot be reached by the shear distortions investigated here; rather, the particle density in strings along $\hat{V}$ must be decreased in favor of more, properly positioned strings. In some of our experiments we observe a flickering in the diffraction pattern at low shear. The frequency of the flickering increases with increasing shear and supports our model for the alternating twin crystal flow. However, this flickering is not always reproducible and may indicate a polycrystalline structure extending along $\hat{\nabla}$ as well as that along $\hat{e}$. The drag mechanism which breaks the crystal up along $\hat{e}$ may also operate along $\hat{\nabla}$ if the relative motion between particles and solvent becomes too large.

The in-plane friction factor Γ' is left as a parameter in the theory and must depend on the size of individual crystallites parallel to the $\hat{e}$ direction. We have presented numerical results for $\mathscr{A} = 1$ which implies $\Gamma = \Gamma'$. For this

$\mathscr{A}$ value at limiting small rates of shear, the most probable δ_2 value is nearly the smallest possible value for the model potential given in Eq. (3.8). This value is approximately constant for $\mathscr{A} < 1$ and increases for $\mathscr{A} > 1$. For $\mathscr{A} = 1$ the minimum δ_2 value corresponds with the experimentally measured distortion at limiting small rates of shear. Differences between the model potential and the true bcc potential will undoubtedly affect the agreement between predicted and measured values of δ_2. However, we have compared the theoretical minimum and most probable values of δ_2 for $\mathscr{A} = 1$ with experimentally measured distortions (most probable experimental values). This comparison is presented in Fig. 10. The fit between theory and experiment determines $\mathscr{B}$ and consequently the effective particle charge, if we assume $\delta_1 = 0$ and $\kappa a = 1$. We have also assumed that the potential barrier height between the bcc twin structures is the same for the model potential and the screened Coulomb potential calculation. The charge we find is $Z \cong 360$ and is in good agreement with that expected experimentally. This result supports our model which takes a different point of view than defect mediated flow.

The assumption that $\kappa a = 1$ is not critical because the maximum in the configurational potential energy presented in Fig. 6 varies by 25% over the stable range of κa. The chosen value is representative. We have chosen $\delta_1 = 0$, because this variable represents a crystal strain which will also be damped by the solvent. Furthermore, layers of alternating bcc twin structures will produce opposing stresses tending to limit $\delta_1 = 0$ as the system is sheared. Thus δ_1 is taken to be zero.

A prediction of this model is that the shear viscosity should decrease with increasing shear. Shear thinning has been observed in colloidal suspensions;[8,21] but for suspensions as dilute as these, shear viscosity measurements are difficult. However, ion exchange-resin beads become trapped in the colloidal solid if they are small in diameter and settle to the bottom if they are large. These phenomena suggest a shear-thinning behavior. Shear-thinning behavior may also be responsible for the spot doubling seen in the rocking-cuvette cell at low rates of shear. The low shear region in the cell center will have a large viscosity and plug flow may develop. A high shear region near the cell walls produces one set of spots and the plug another. The shear-thinning behavior is qualitatively the same as predicted by Evans for the soft-sphere fluid system. However, the force F is directly related to the intrinsic stress or pressure tensor for the colloidal particles and this function decreases with increasing shear in opposition to the prediction for a pure soft-sphere fluid. However, one system is a pure fluid and the other is a suspension. This study looks at low shear near the solid phase, while Evans's study extends to correspondingly larger rates of shear.

The shear-induced distortions predicted for pure fluids[24] and used for colloidal liquids[5] expands the pair distribution function about the equilibrium pair distribution function. For the model presented in this paper the most probable state of the system is not located at the equilibrium position. Rather it is near the position of maximum force on the appropriate trajectory. If this position can be determined, it is a better point of expansion for theoretical analysis. Whether this behavior is related to nonanalytic behavior of transport properties remains to be seen.

One may question the adequacy of a "single crystal" description of the shear flow. The shear flow might break the crystal into a large number of independent slabs which freely slip past one another. As the shear increases the slab thickness decreases and the slabs gradually relax to the 2D hcp structure. This would be supported by experimental observation, but the previously discussed calculations indicate a different behavior. Theoretically the slabs would not exhibit much internal relaxation until they were one or two layers thick. Then the relaxation would be nearly complete. One would expect to see a rapid change from bcc to hcp or a coexistence of the two structures, as a function of the shear rate. This is not seen experimentally.

Finally, packing arguments appear to be a key to understanding the shearing process in bcc crystals. The $\langle 111 \rangle$ directions are the closest packed directions and the (110) planes are the closest packed planes. Stressed bcc crystals will slip along these directions. In a shear flow colloidal crystals orient with a $\langle 111 \rangle$ direction parallel to the velocity of the flow with (110) planes perpendicular to the shear. Increasing the rate of shear distorts (110) layers as discussed in this paper, but the $\langle 111 \rangle$ direction is unaffected in packing. Larger rates of shear break up the (110) layers, but strings of particles are still directed along the flow direction. Finally the strings break up leaving an amorphous structure at very large rates of shear.

ACKNOWLEDGMENTS

B. J. Ackerson thanks Heinz Hall for the design of the quartz disk cell. The support of this work by the National Science Foundation (Division of Materials Research, Low Temperature Physics Program) Grants No. DMR-81-16119 for B.J.A. and No. DMR-82-06472 for N.A.C. is gratefully acknowledged.

[1]R. M. Fitch, *Polymer Colloids* (Plenum, New York, 1971).
[2]P. Pieranski, Contemp. Phys. **24**, 25 (1983).
[3]P. N. Pusey and R. J. A. Tough, in *Dynamic Light Scattering and Velocimetry*, edited by R. Pecora (Plenum, New York, in press).
[4]W. D. Dozier and P. M. Chaikin, J. Phys. (Paris) **43**, 843 (1982).
[5]N. A. Clark and B. J. Ackerson, Phys. Rev. Lett. **44**, 1005 (1980).
[6]B. J. Ackerson and N. A. Clark, Phys. Rev. Lett. **46**, 123 (1981).
[7]B. J. Ackerson and N. A. Clark, Physica (Utrecht) A **118**, 221

(1983).
[8]R. L. Hoffman, Trans. Soc. Rheol. **16**, 155 (1972); J. Colloid Interface Sci. **46**, 491 (1974).
[9]N. A. Clark, A. J. Hurd, and B. J. Ackerson, Nature **281**, 57 (1979).
[10]W. T. Ashurst and W. G. Hoover, Phys. Rev. A **11**, 658 (1975).
[11]D. J. Evans, Physica (Utrecht) A **118**, 51 (1983).
[12]S. Hess and H. J. M. Hanley, Phys. Rev. A **25**, 1801 (1982).
[13]D. J. Evans, Physica (Utrecht) A **25**, 2788 (1982).
[14]K. Kawasaki and J. D. Gunton, Phys. Rev. A **8**, 2048 (1973).
[15]R. E. Reed-Hill, *Physical Metallurgy Principles* (Van Nostrand, Princeton, 1968), Chap. 4.
[16]B. J. Ackerson and N. A. Clark, J. Phys. (Paris) **42**, 929 (1981).
[17]G. S. Manning, J. Chem. Phys. **51**, 924 (1969).
[18]J. Silva and B. J. Mokross, Phys. Rev. B **21**, 2927 (1980).
[19]L. L. Foldy, Phys. Rev. B **3**, 3473 (1973).
[20]S. Marcelja, D. J. Mitchell, and B. W. Ninham, Chem. Phys. Lett. **43**, 353 (1976).
[21]H. M. Lindsay and P. M. Chaikin, J. Chem. Phys. **76**, 3774 (1982).
[22]P. P. Ewald, Ann. Phys. (Leipzig) **64**, 253 (1921).
[23]B. E. Warren, *X-Ray Diffraction* (Addison-Wesley, Reading, Mass., 1969), p. 305.
[24]H. S. Green, *The Molecular Theory of Liquids* (Dover, New York, 1969), p. 315ff.

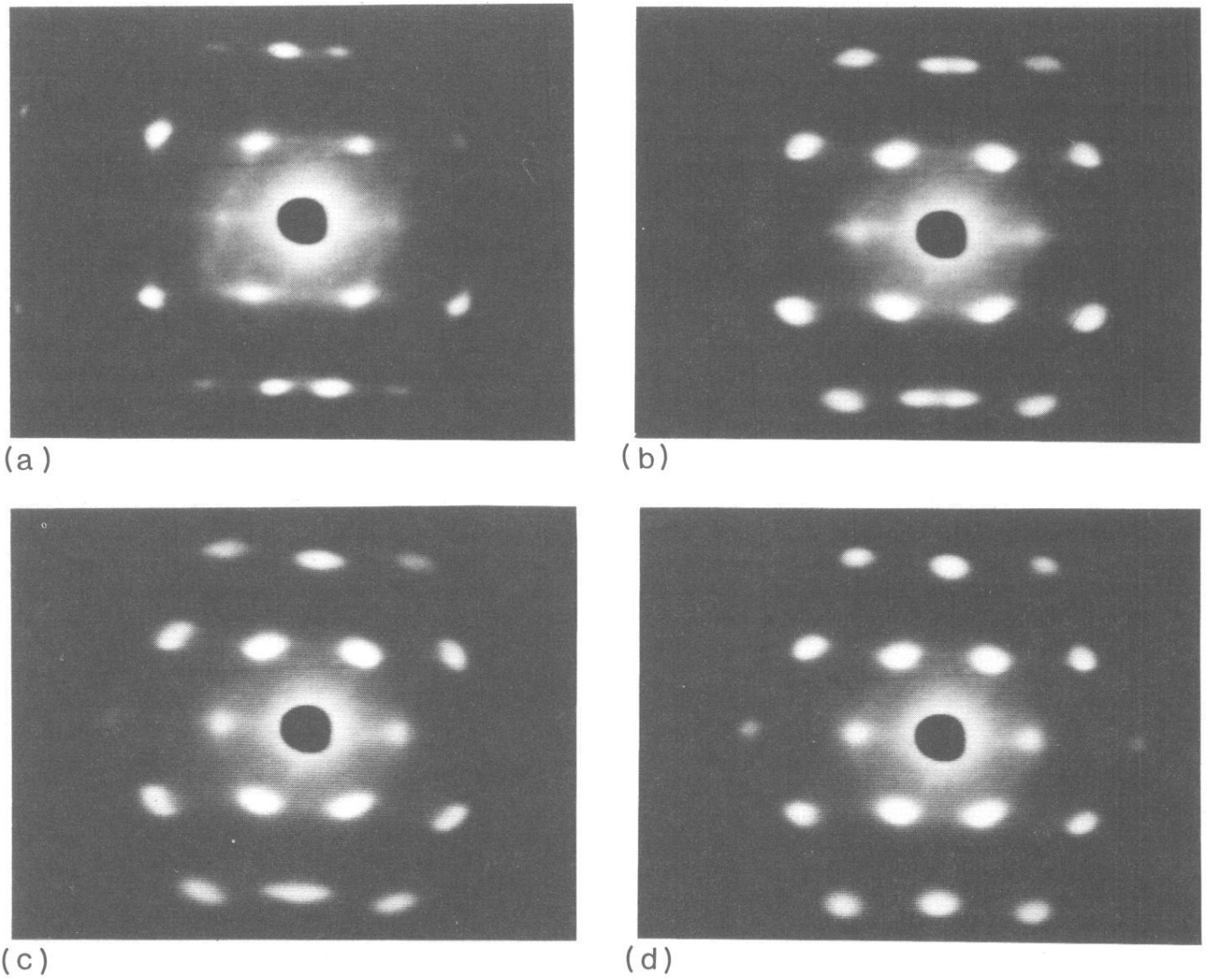

FIG. 2. Photographs of video records made of scattering intensity distributions produced by a 0.17 wt. % deionized aqueous suspension of 0.220-μm-diameter polystyrene particles. At zero shear a bcc twin structure is identified in (a). The visible lines are due to thermal diffuse scattering. For small rates of shear ($\hat{V}$ upward and $\hat{\nabla}$ normal to the plane of the page), the Laue spots are observed to shift horizontally toward a vertical axis, which passes through the k-space origin at the beam stop (center). This shift is proportional to the $\hat{k}_v$ component of a given reciprocal-lattice point and increases with increasing rate of shear. In (b) there are two sets of 211 spots, which have merged in (c) and continue to merge in (d) as the rate of shear is increased. In (d) the shear rate (~ 10 Hz) is sufficiently large that the original bcc structure now looks like a distorted 2D hcp structure.